THEMIS Observations of the Magnetopause Electron Diffusion Region: Large Amplitude Waves and Heated Electrons

Xiangwei Tang,[1] Cynthia Cattell,[1] John Dombeck,[1] Lei Dai,[1] Lynn B. Wilson III,[2] Aaron Breneman,[1] Adam Hupach[1]

We present the first observations of large amplitude waves in a well-defined electron diffusion region at the sub-solar magnetopause using data from one THEMIS satellite. These waves identified as whistler mode waves, electrostatic solitary waves, lower hybrid waves and electrostatic electron cyclotron waves, are observed in the same 12-sec waveform capture and in association with signatures of active magnetic reconnection. The large amplitude waves in the electron diffusion region are coincident with abrupt increases in electron parallel temperature suggesting strong wave heating. The whistler mode waves which are at the electron scale and enable us to probe electron dynamics in the diffusion region were analyzed in detail. The energetic electrons (∼30 keV) within the electron diffusion region have anisotropic distributions with $T_{e\perp}/T_{e\parallel} > 1$ that may provide the free energy for the whistler mode waves. The energetic anisotropic electrons may be produced during the reconnection process. The whistler mode waves propagate away from the center of the 'X-line' along magnetic field lines, suggesting that the electron diffusion region is a possible source region of the whistler mode waves.

1. Introduction

Magnetic reconnection is considered to be an important energy conversion process [*Dungey*, 1961] that occurs in a variety of plasma environments. At the Earth's magnetopause, it facilitates the entry of solar wind plasma and electromagnetic energy into the magnetosphere. Reconnection sites are regions of strong wave activity covering a broad range of frequencies. Wave modes frequently observed near reconnection sites include the whistler mode (WH) waves [*Deng and Matsumoto*, 2001; *Petkaki et al.*, 2006], electrostatic solitary waves (ESWs) [*Farrell et al.*, 2002; *Matsumoto et al.*, 2003], lower hybrid (LH) waves [*Cattell and Mozer*, 1986; *Bale et al.*, 2002], kinetic *Alfvén* waves [*Chaston et al.*, 2005] and Langmuir/upper hybrid waves [*Farrell et al.*, 2002]. The effect of different wave modes on the reconnection process has been a problem of longstanding interest - for their role in anomalous resistivity, particle acceleration, energy transport and formation of reconnection sites [*Huba et al.*, 1977; *Labelle and Treumann*, 1988; *Treumann et al.*, 1991; *Drake et al.*, 2003].

[1]School of Physics and Astronomy, University of Minnesota, Minneapolis, Minnesota, USA.

[2]Goddard Space Flight Center, Heliospheric Physics Laboratory, Greenbelt, Maryland, USA.

0094-8276/13/$5.00

Observations of the electron diffusion region (EDR) have been made by Polar at the subsolar magnetopause [*Mozer et al.*, 2002], by Wind in the magnetotail [*Øieroset et al.*, 2002] and by Cluster in the magnetosheath [*Phan et al.*, 2007]. Recent simulations and observations of EDRs during collisionless antiparallel reconnection in Earth's magnetotail [*Ng et al.*, 2011] report that the diffusion region is characterized by a narrow extended layer containing electron jets. It is shown that the jets in the layer are driven by electron pressure anisotropy $P_{e\parallel} >> P_{e\perp}$ and the anisotropy is responsible for the structure of the EDR [*Ng et al.*, 2011]. *Mozer* [2005] has identified EDRs on the basis of the nonzero parallel electric field, a large perpendicular electric field compared to the reconnection electric field, a large electromagnetic energy conversion rate and accelerated electrons, and a topological boundary that separates regions having different $\mathbf{E} \times \mathbf{B}/B^2$ flows with thickness of the order of the electron skin depth. In this paper, we concentrate on a specific way to identify the EDR described by *Scudder et al.* [2012] who report spatially resolved diagnostic signatures of a demagnetized EDR observed by Polar at the Earth's magnetopause. The five dimensionless scalar diagnostics that were used to find the EDR are peak electron thermal Mach numbers $M_{e\perp} \equiv \frac{|\mathbf{U}_e|}{<w_{e\perp}>} > 1.5$ where $\mathbf{U}_e$ represents electron bulk velocity and $< w_{e\perp} >$ is the electron thermal speed derived from the average perpendicular temperatures, electron temperature anisotropy $An_e \equiv \frac{T_{e\parallel}}{<T_{e\perp}>} > 7$, calibrated agyrotropy of electron pressure tensor $A\phi_e = 2\frac{|1-\alpha|}{(1+\alpha)} > 1$ where $\alpha \equiv P_{e\perp,1}/P_{e\perp,2}$, expansion parameters of guiding center theory indicative of demagnetization and strong $(150eV)$ increases in electron temperature [*Scudder et al.*, 2012].

This paper focuses on the WH waves which are an important candidate for the anomalous resistivity, particle acceleration and heating. WH waves may be driven unstable by superthermal electrons with temperature anisotropies of $T_{e\perp}/T_{e\parallel} > 1$ in the magnetosphere [*Kennel and Petschek*, 1966] and current-driven plasma instabilities [*Gurnett et al.*, 1976] or energetic electron beams [*Zhang et al.*, 1999] in the magnetotail. WH waves are one of the most ubiquitous wave modes observed in space plasmas. Observations of WH waves at the Earth's magnetopause have been made by *Deng and Matsumoto* [2001]. Electron anisotropy, due to compression of the magnetopause or LH drift waves, may be the generation mechanism of WH waves in the magnetopause current sheet [*Karimabadi et al.*, 2004]. WH waves in the EDR may play a significant role in the microphysics of reconnection as they are excited on electron scales. It is believed that WH waves in the magnetopause current sheet may affect the instability of the current sheet to reconnection via tearing. The generation of the out-of-plane component of the magnetic field is suggested to be a signature of whistler mediated reconnection [*Mandt et al.*, 1994]. It has also been suggested that the strongest whistler emissions are observed on the most recently opened magnetospheric flux tubes due to magnetic reconnection [*Vaivads et al.*, 2007]. One recent simulation study concludes that WH waves do

not control the dissipation processes of reconnection but are generated as a result of the reconnection processes [*Fujimoto and Sydora*, 2008]. In this paper, we present an example of a reconnection event at the sub-solar magnetopause observed by THEMIS. In section 2, we describe the data sets and analysis techniques. In section 3, we show the observations. Finally, we discuss the conclusions of our study in section 4.

2. Data Sets and Analysis

The THEMIS mission consists of five identically-instrumented spacecraft [*Angelopoulos*, 2008]. The Electric Field Instrument (EFI) measures three components of the electric field [*Bonnell et al.*, 2008]. The instrument provides continuous coverage at 128 samples/s in survey mode and waveform captures at 8192 samples/s in wave burst mode. The Magnetic Fields Experiment (MFE) includes a Flux Gate Magnetometer (FGM) which measures DC magnetic field with a sampling rate of 128 samples/s in the high rate mode or 4 samples/s in the low rate mode [*Auster et al.*, 2008] and a Search Coil Magnetometer (SCM) which measures magnetic fluctuations sampled at 8192 samples/s in the burst mode [*Roux et al.*, 2008; *Le Contel et al.*, 2008]. Particle data are measured by the Electrostatic Analyzer (ESA) [*McFadden et al.*, 2008] and by the Solid State Telescope (SST) [*Angelopoulos*, 2008]. The ESA measures plasma over the energy range of a few eV up to 30 keV for electrons and 25 keV for ions. The SST measures the distribution functions of superthermal particles within the energy range from 25 keV to 6 MeV for electrons and 900 keV for ions. Because the measured quasi-static electric field component along the spin axis has large uncertainty due to the short boom along the spin axis we use $\mathbf{E}\cdot\mathbf{B} = 0$ to determine the electric field used to calculate the $\mathbf{E} \times \mathbf{B}/B^2$ velocity. The coordinate systems used in this paper include geocentric solar magnetospheric (GSM) coordinates and field-aligned coordinates (FAC). The FAC is defined in the following way: The positive Z axis points in the direction of the magnetic field at the spacecraft's location. The positive X axis lies in the plane of the magnetic field line passing through the spacecraft's location, perpendicular to the Z axis, and points inwards (towards the inside of the field line). The positive Y axis completes the orthogonal right-handed system. Waveforms are analyzed dynamically in time and frequency using Morlet wavelet transform [*Torrence and Compo*, 1998]. The wave vector is determined using Minimum Variance Analysis (MVA) [*Khrabrov and Sonnerup*, 1998] on bandpass filtered three magnetic field components.

3. Observations

Figure 1 shows a 7-min interval of the field and plasma observations made by probe E of the THEMIS mission on August 27, 2009. The boundary normal direction (determined from MVA on the ambient magnetic field) was [0.99, 0.015, -0.12] in GSM coordinates and almost identical to the GSM-X direction, consistent with the spacecraft being near the sub-solar point (indicated by the position parameters at the bottom of Figure 1). The spacecraft travels from the outer magnetosphere (SP) through the magnetopause (MP, indicated by two light green shaded bands) into the magnetosheath (SH). The purple shaded band shows an ∼12-sec interval of magnetic burst data capture.

The magnetopause crossing can be seen in the change in Bz from positive to negative in Panel A of Figure 1. The differential energy flux of electrons in Panel K shows that in the magnetosphere, where Bz was positive, high-energy electrons were encountered; while in the magnetosheath, where Bz was negative, lower-energy electrons were measured. The spacecraft passed from the lower plasma density mangetosphere to the higher density (factor of 100) magnetosheath via a region of mixed magnetosheath/magnetospheric plasmas comprising the low latitude boundary layer as shown in Panel H. This observation is evidence for the transport of solar wind plasma across the magnetopause. The presence of accelerated plasma flow is seen through the magnetopause current sheet as shown in Panels D and E. The spacecraft crossed the magnetopause south of the separator, as suggested by the negative GSM-Z component of ion flow velocity and the result of Walen test [*Sonnerup et al.*, 1981]. Based on the prediction of the magnetopause reconnection model being a rotational discontinuity [*Paschmann et al.*, 1979], the Walen test [*Sonnerup et al.*, 1981] states that the observed flow velocity change between a point in the magnetopause and a reference point in the adjacent magnetosheath equals the predicted modified Alfven velocity change. The angle deviations between the observations and the prediction are almost 180° for this event. This anti-parallel relation indicates that the spacecraft crossed south of the separator [*Sonnerup et al.*, 1981]. The encounter with the magnetopause current sheet is associated with fast ion jetting consistent with the Walen relation and fast electron flows, indicating that reconnection is occurring. Magnetic reconnection is generally considered to be the primary mechanism through which transport of plasma and energy across the magnetopause occurs.

3.1. Identification of EDR

Enhanced wave activity can be seen associated with the magnetopause crossing from Panels A (ambient magnetic field), B (burst magnetic field) and C (electric fluctuations). We note that the electric fluctuations maximize during the magnetic burst interval. During this interval, electron flow speed (Panel E), anisotropy, agyrotropy and Mach number (Panel J) also maximize. These enhanced amplitudes are coincident with abrupt increases in electron parallel temperature $T_{e\|}$ shown in Panel I suggesting strong wave heating. As will be discussed in more detail in next section, the observed intense waves may provide the observed electron heating. All these features, along with the fact that the electron perpendicular flow velocity is not consistent with the $\mathbf{E}\times\mathbf{B}/B^2$ velocity during the magnetic burst interval (Panel G), provide evidence for the detection of an EDR. Another feature is the density depletion shown in Panel H (purple shaded band) which might indicate the center of the EDR. These signatures are consistent with the simulation and observations of *Scudder et al.* [2012]. Panels L and M show the electron pitch angle spectra for lower engery electrons measured by ESA and higher energy electrons measured by SST, respectively. The magnetic field (Panel A) and electric field (Panel C) fluctuations enhance in the magnetopause boundary layer and in the magnetosheath with field-aligned and counter-streaming lower energy electrons as shown in Panel L. However, the higher energy electron pitch angle (Panel M) enhances around 90° in the boundary layer and in the magnetosheath, especially during the purple shaded magnetic burst interval. Distinct from the electron distributions in the boundary layer and in the magnetosheath, the higher energy electron pitch angle enhances at 0° and 180° and the lower energy electrons are more isotropic near the current sheet center around 15:36:00 UT and 15:37:00 UT.

3.2. Observations of waves

Figure 2 shows an example of the identified WH waves at the time indicated by a black vertical line in Panel B of Figure 1. It can be seen from Panels A and B of Figure 2 that the waves have frequencies from 0.1 to 0.6 f_{ce} (electron cyclotron frequency) with amplitudes up to 3 nT (peak-peak). As can be seen from Panel C, the wave Poynting flux is mostly anti-parallel to the ambient magnetic field. The wave vector ($k = [-0.23, -0.09, 0.97]$ in FAC), determined from MVA on bandpass filtered wave magnetic field, is nearly along the background magnetic field. The wave propagation angle with respect to the ambient magnetic field θ_{kB} is determined as $\sim 166^\circ$ since the Poynting flux is mostly anti-parallel to the magnetic field. An expanded view of the WH waves can be seen in Panels D and E which respectively show the filtered (200-2000 Hz) waveforms of the burst magnetic and electric field data over the time interval indicated by the purple bar in Panel A. Panel F shows that the WH waves are circularly right-handed polarized with respect to the ambient magnetic field as expected. The electron distribution functions observed at times close to and/or concurrently with the WH waves are shown in Panels G and H. The lower energy electrons (∼100 eV) shown in Panel G have anisotropic distributions with $T_{e\perp}/T_{e\|} < 1$. However, the energetic electrons (∼30 keV) shown in Panel H have anisotropic distributions with a larger population moving in perpendicular direction. Broad-banded emissions with strong electric (∼10 mV/m) and magnetic (∼40 nT) field fluctuations below ion cyclotron frequency (∼1 Hz) and electric (∼30 mV/m) and magnetic (∼20 nT) field fluctuations below LH frequency (∼30 Hz) are also detected during this magnetopause crossing (not shown). These intense wave emissions may provide the observed electron heating associated with the magnetopause crossing.

Figure 3 shows examples of electrostatic waves at a time preceding the waves in Figure 2 by 0.05 seconds. WH waves at a frequency of $\sim 0.3 f_{ce}$ are observed in the magnetic fluctuations in Panel A from 15:35:33.650 UT to 15:35:33.700 UT. This time interval overlaps with that of the ESWs, suggesting a possible coupling of WH waves and ESWs. ESWs (up to 30 mV/m) indicated by the magenta arrows in Panel B have a broad spectrum which extends from 200 Hz to 3000 Hz shown in Panel C. The high-frequency electrostatic waves (up to 35 mV/m) labeled by light blue arrows in Panel B have power that peaks at f_{ce}, which can be seen from both the wavelet power spectrum in Panel C and the Fourier power in Panel G. During this time interval, there is no power in the wave magnetic field at f_{ce} (not shown). This wave mode is linearly polarized, as shown in the hodograms in Panels D, E, and F in FAC with an interval indicated by the light blue arrows below Panel C. Occasionally these high-frequency emissions are seen associated with clear harmonics, possibly suggesting electrostatic electron cyclotron (EEC) waves.

4. Discussion and Conclusions

We have presented the first observations of intense waves in the EDR in a sub-solar magnetopause reconnection region. The identification of the EDR in this event is based on the occurrence of signatures of strong electron heating, large electron thermal anisotropy, agyrotropy and Mach number and electron velocity not consistent with the $\mathbf{E} \times \mathbf{B}$ velocity, consistent with the simulation and observations of *Scudder et al.* [2012]. The lower energy electrons (∼100 eV) with anisotropic distributions of $T_{e\perp}/T_{e\|} < 1$ within the EDR may have been heated by the observed waves with frequency below the LH frequency, consistent with the suggestion that LH waves lead to electron heating in the parallel direction [*Cairns and McMillan*, 2005].

We identified intense WH waves inside the EDR. This is inconsistent with reported simulation results that indicated WH waves are only driven downstream of an EDR [*Fujimoto and Sydora*, 2008]. The WH waves seen by THEMIS in the EDR propagate almost anti-parallel to the ambient magnetic field and the Poynting flux indicates that the WH waves propagate away from the center of the 'X-line' along magnetic field lines. The observed electron temperature anisotropy of $T_{e\perp}/T_{e\|} > 1$ for energies above 20keV may be the source of free energy for the generation of the WH waves. The energetic electron anisotropy may be produced by adiabatic heating in the perpendicular direction as the locally intensified magnetic field can accelerate electrons in the perpendicular direction [*Fujimoto and Sydora*, 2008]. On the field lines directly connected to the EDR, the energetic electron anisotropy may also be due to high energy field-aligned electrons (accelerated by the reconnection process) being lost to the magnetosheath [*Stenberg et al.*, 2005]. WH waves can scatter the electrons in pitch-angle distribution and relax the temperature anisotropy. Studies of large amplitude whistlers in the inner magnetosphere have provided evidence for rapid scattering and/or energization [*Cattell et al.*, 2008]. WH waves may play a significant role in the microphysics of reconnection through the enabling of a current sheet instability, the decoupling of electrons, the acceleration and heating of particles, and the transport of energy away from the reconnection region.

A possible coupling of EEC waves and ESWs with WH waves is often seen during magnetopause reconnection. The growth of the electrostatic waves may reduce the electron temperature anisotropy and reduce the growth rate of WH waves. The physics of wave coupling process is important to understand the effect of wave-wave interactions on the reconnection process and will be investigated in a future study. This study provides further evidence that the plasma waves can play a significant role in the microphysics of magnetic reconnection at the Earth's magnetopause.

Acknowledgments. At the University of Minnesota, this work was supported by NNX08AF28 and a contract from APL for the development of RBSP/EFW. The authors acknowledge NASA contract NAS5-02099 and V. Angelopoulos for use of data from the THEMIS Mission, specifically: J. W. Bonnell and F. S. Mozer for use of EFI data; D. Larson and R. P. Lin for use of SST data; C. W. Carlson and J. P. McFadden for use of ESA data; A. Roux and O. LeContel for use of SCM data; and K. H. Glassmeier, U. Auster and W. Baumjohann for the use of FGM data provided under the lead of the Technical University of Braunschweig and with financial support through the German Ministry for Economy and Technology and the German Center for Aviation and Space (DLR) under contract 50 OC 0302. The authors are grateful for discussion and comments from S. Thaller, K. Kersten and C. Colpitts.

References

Angelopoulos, V. (2008), The THEMIS Mission, *Space Sci. Rev.*, *141*, 5–34, doi:10.1007/s11214-008-9336-1.

Auster, H. U., et al. (2008), The THEMIS Fluxgate Magnetometer, *Space Sci. Rev.*, *141*, 235–264, doi:10.1007/s11214-008-9365-9.

Bale, S. D., F. S. Mozer, and T. Phan (2002), Observation of lower hybrid drift instability in the diffusion region at a reconnecting magnetopause, *Geophys. Res. Lett.*, *29*(24), 2180, doi:10.1029/2002GL016113.

Bonnell, J. W., F. S. Mozer, G. T. Delory, A. J. Hull, R. E. Ergun, C. M. Cully, V. Angelopoulos, and P. R. Harvey (2008), The Electric Field Instrument (EFI) for THEMIS, *Space Sci. Rev.*, *141*, 303–341, doi:10.1007/s11214-008-9469-2.

Cairns, I. H., and B. F. McMillan (2005), Electron acceleration by lower hybrid waves in magnetic reconnection regions, *Physics of Plasmas*, *12*(10), 102,110, doi:10.1063/1.2080567.

Cattell, C., et al. (2008), Discovery of very large amplitude whistler-mode waves in Earth's radiation belts, *Geophys. Res. Lett.*, *35*, L01105, doi:10.1029/2007GL032009.

Cattell, C. A., and F. S. Mozer (1986), Experimental determination of the dominant wave mode in the active near-earth magnetotail, *Geophys. Res. Lett.*, *13*(3), 221–224, doi:10.1029/GL013i003p00221.

Chaston, C. C., et al. (2005), Drift-Kinetic Alfvén Waves Observed near a Reconnection X Line in the Earth's Magnetopause, *Phys. Rev. Lett.*, *95*(6), 065002, doi:10.1103/PhysRevLett.95.065002.

Deng, X. H., and H. Matsumoto (2001), Rapid magnetic reconnection in the Earth's magnetosphere mediated by whistler waves, *Nature*, *410*, 557–560, doi:10.1038/35069018.

Drake, J. F., M. Swisdak, C. Cattell, M. A. Shay, B. N. Rogers, and A. Zeiler (2003), Formation of Electron Holes and Particle Energization During Magnetic Reconnection, *Science*, *299*, 873–877, doi:10.1126/science.1080333.

Dungey, J. W. (1961), Interplanetary Magnetic Field and the Auroral Zones, *Phys. Rev. Lett.*, *6*, 47–48, doi:10.1103/PhysRevLett.6.47.

Farrell, W. M., M. D. Desch, M. L. Kaiser, and K. Goetz (2002), The dominance of electron plasma waves near a reconnection X-line region, *Geophys. Res. Lett.*, *29*(19), 1902, doi:10.1029/2002GL014662.

Fujimoto, K., and R. D. Sydora (2008), Whistler waves associated with magnetic reconnection, *Geophys. Res. Lett.*, *35*, L19112, doi:10.1029/2008GL035201.

Gurnett, D. A., L. A. Frank, and R. P. Lepping (1976), Plasma waves in the distant magnetotail, *J. Geophys. Res.*, *81*, 6059–6071, doi:10.1029/JA081i034p06059.

Huba, J. D., N. T. Gladd, and K. Papadopoulos (1977), The lower-hybrid-drift instability as a source of anomalous resistivity for magnetic field line reconnection, *Geophys. Res. Lett.*, *4*, 125–126, doi:10.1029/GL004i003p00125.

Karimabadi, H., W. Daughton, and K. B. Quest (2004), Role of electron temperature anisotropy in the onset of magnetic reconnection, *Geophys. Res. Lett.*, *31*, L18801, doi:10.1029/2004GL020791.

Kennel, C. F., and H. E. Petschek (1966), Limit on Stably Trapped Particle Fluxes, *J. Geophys. Res.*, *71*, 1.

Khrabrov, A. V., and B. U. Ö. Sonnerup (1998), Error estimates for minimum variance analysis, *J. Geophys. Res.*, *103*, 6641–6652, doi:10.1029/97JA03731.

Labelle, J., and R. A. Treumann (1988), Plasma waves at the dayside magnetopause, *Space Sci. Rev.*, *47*, 175–202, doi:10.1007/BF00223240.

Le Contel, O., et al. (2008), First Results of the THEMIS Search Coil Magnetometers, *Space Sci. Rev.*, *141*, 509–534, doi:10.1007/s11214-008-9371-y.

Mandt, M. E., R. E. Denton, and J. F. Drake (1994), Transition to whistler mediated magnetic reconnection, *Geophys. Res. Lett.*, *21*, 73–76, doi:10.1029/93GL03382.

Matsumoto, H., X. H. Deng, H. Kojima, and R. R. Anderson (2003), Observation of Electrostatic Solitary Waves associated with reconnection on the dayside magnetopause boundary, *Geophys. Res. Lett.*, *30*(6), 1326, doi:10.1029/2002GL016319.

McFadden, J. P., C. W. Carlson, D. Larson, M. Ludlam, R. Abiad, B. Elliott, P. Turin, M. Marckwordt, and V. Angelopoulos (2008), The THEMIS ESA Plasma Instrument and In-flight Calibration, *Space Sci. Rev.*, *141*, 277–302, doi:10.1007/s11214-008-9440-2.

Mozer, F. S. (2005), Criteria for and statistics of electron diffusion regions associated with subsolar magnetic field reconnection, *J. Geophys. Res.*, *110*, A12222, doi:10.1029/2005JA011258.

Mozer, F. S., S. D. Bale, and T. D. Phan (2002), Evidence of Diffusion Regions at a Subsolar Magnetopause Crossing, *Phys. Rev. Lett.*, *89*(1), 015002, doi:10.1103/PhysRevLett.89.015002.

Ng, J., J. Egedal, A. Le, W. Daughton, and L.-J. Chen (2011), Kinetic Structure of the Electron Diffusion Region in Antiparallel Magnetic Reconnection, *Phys. Rev. Lett.*, *106*(6), 065002, doi:10.1103/PhysRevLett.106.065002.

Øieroset, M., R. P. Lin, T. D. Phan, D. E. Larson, and S. D. Bale (2002), Evidence for Electron Acceleration up to ˜300 keV in the Magnetic Reconnection Diffusion Region of Earth's Magnetotail, *Phys. Rev. Lett.*, *89*(19), 195001, doi:10.1103/PhysRevLett.89.195001.

Paschmann, G., et al. (1979), Plasma acceleration at the earth's magnetopause - Evidence for reconnection, *nature*, *282*, 243–246, doi:10.1038/282243a0.

Petkaki, P., M. P. Freeman, and A. P. Walsh (2006), Cluster observations of broadband electromagnetic waves in and around a reconnection region in the Earth's magnetotail current sheet, *Geophys. Res. Lett.*, *33*, L16105, doi:10.1029/2006GL027066.

Phan, T. D., J. F. Drake, M. A. Shay, F. S. Mozer, and J. P. Eastwood (2007), Evidence for an elongated (> 60 ion skin depths) electron diffusion region during fast magnetic reconnection, *Phys. Rev. Lett.*, *99*, 255,002, doi:10.1103/PhysRevLett.99.255002.

Roux, A., O. Le Contel, C. Coillot, A. Bouabdellah, B. de La Porte, D. Alison, S. Ruocco, and M. C. Vassal (2008), The Search Coil Magnetometer for THEMIS, *Space Sci. Rev.*, *141*, 265–275, doi:10.1007/s11214-008-9455-8.

Scudder, J. D., R. D. Holdaway, W. S. Daughton, H. Karimabadi, V. Roytershteyn, C. T. Russell, and J. Y. Lopez (2012), First Resolved Observations of the Demagnetized Electron-Diffusion Region of an Astrophysical Magnetic-Reconnection Site, *Phys. Rev. Lett.*, *108*(22), 225005, doi:10.1103/PhysRevLett.108.225005.

Sonnerup, B. U. O., G. Paschmann, I. Papamastorakis, N. Sckopke, G. Haerendel, S. J. Bame, J. R. Asbridge, J. T. Gosling, and C. T. Russell (1981), Evidence for magnetic field reconnection at the earth's magnetopause, *J. Geophys. Res.*, *86*, 10,049–10,067, doi:10.1029/JA086iA12p10049.

Stenberg, G., T. Oscarsson, M. André, A. Vaivads, M. Morooka, N. Cornilleau-Wehrlin, A. Fazakerley, B. Lavraud, and P. M. E. Décréau (2005), Electron-scale sheets of whistlers close to the magnetopause, *Annales Geophysicae*, *23*, 3715–3725, doi:10.5194/angeo-23-3715-2005.

Torrence, C., and G. P. Compo (1998), A Practical Guide to Wavelet Analysis., *Bulletin of the American Meteorological Society*, *79*, 61–78, doi:10.1175/15200477(1998)079.

Treumann, R. A., J. Labelle, and R. Pottelette (1991), Plasma diffusion at the magnetopause - The case of lower hybrid drift waves, *J. Geophys. Res.*, *96*, 16,009, doi:10.1029/91JA01671.

Vaivads, A., O. Santolík, G. Stenberg, M. André, C. J. Owen, P. Canu, and M. Dunlop (2007), Source of whistler emissions at the dayside magnetopause, *Geophys. Res. Lett.*, *34*, L09106, doi:10.1029/2006GL029195.

Zhang, Y., H. Matsumoto, and H. Kojima (1999), Whistler mode waves in the magnetotail, *J. Geophys. Res.*, *104*.

X. Tang, 116 Church Street S.E., Minneapolis, MN, 55455, USA. (xtangphysics@gmail.com)

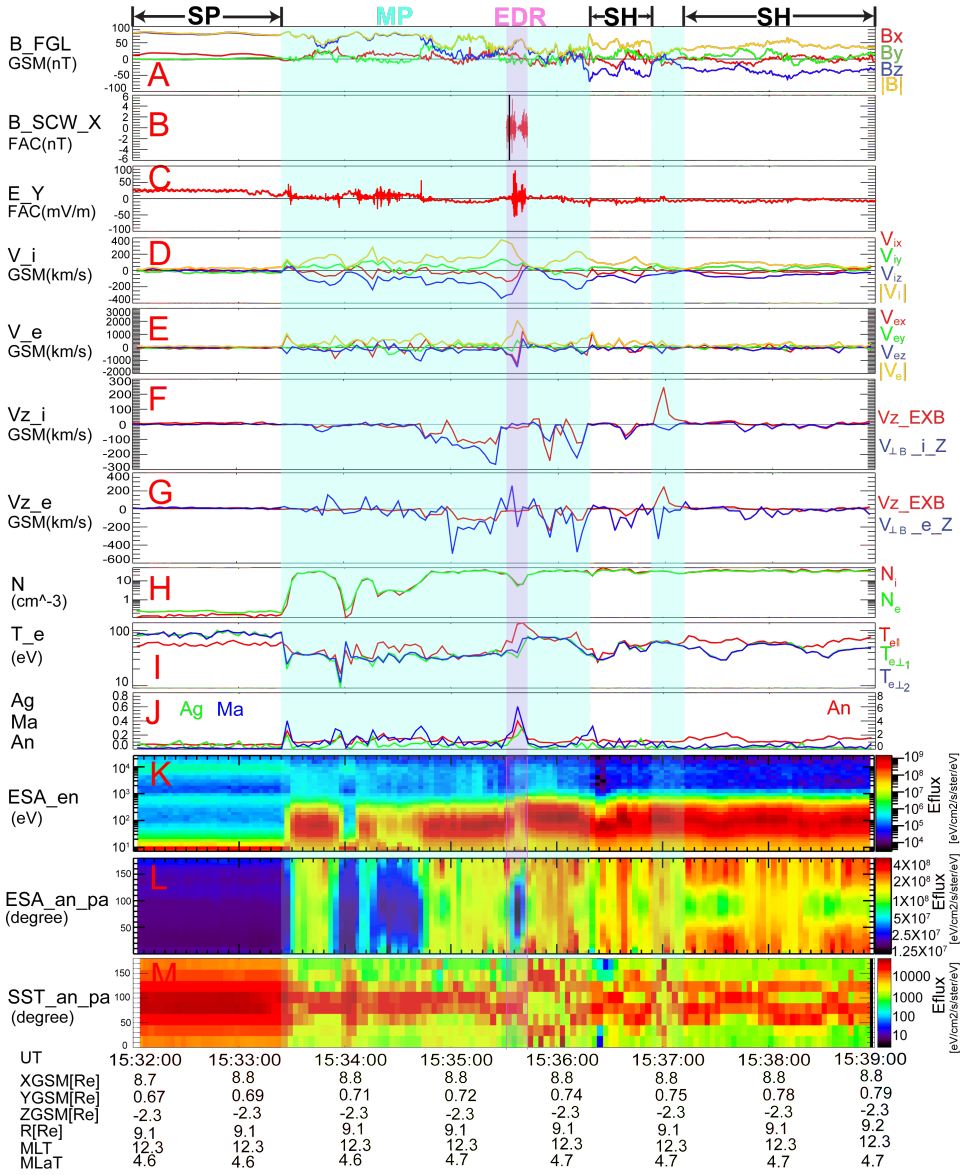

Figure 1. A reconnection event at the sub-solar magnetopause observed by THEMIS-E on August 27, 2009. (A): 4 samples/s magnetic field data in GSM. (B): perpendicular X component of the burst magnetic field at 8192 samples/s in FAC. (C): perpendicular Y component of the electric field at 128 samples/s in FAC. (D) and (E): ion and electron bulk flow velocity in GSM, respectively. (F) and (G): comparisons of GSM-Z component of the $\mathbf{E}\times\mathbf{B}/B^2$ velocity with the GSM-Z component of ion (F) and electron (G) perpendicular flow velocity with respect to the ambient magnetic field, respectively. (H): ion and electron densities. (I): electron temperatures. (J): electron agyrotropy and Mach number (scale to the left) and temperature anisotropy (scale to the right). (K): differential energy flux for electrons measured by ESA. (L) and (M): electron pitch angle spectra for lower engery electrons measured by ESA and higher energy electrons measured by SST, respectively.

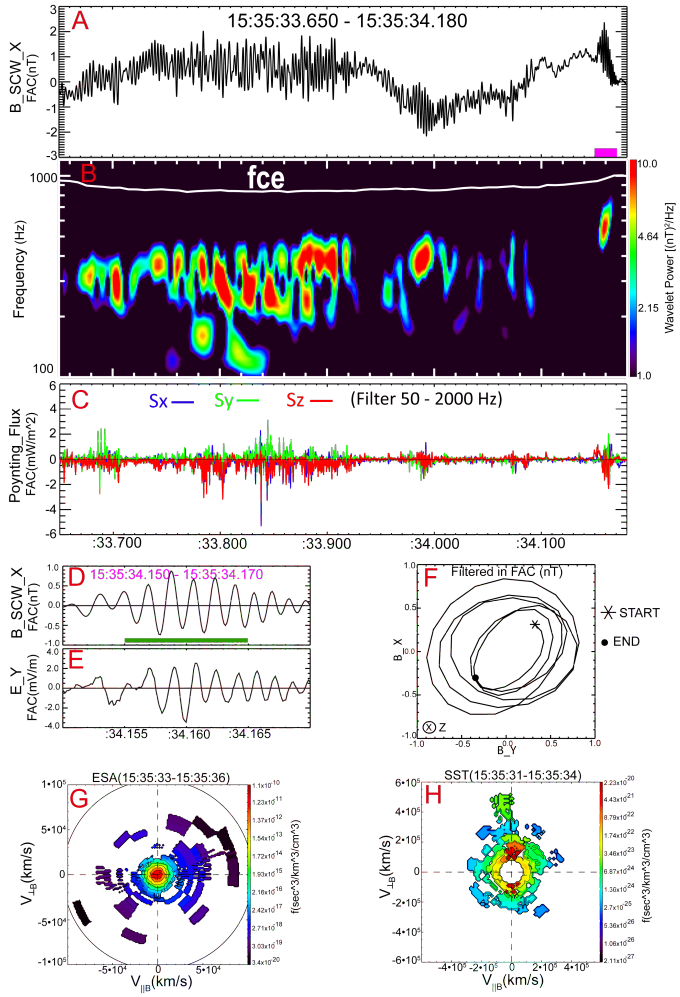

Figure 2. Example of WH waves within the EDR. (A), (B) and (C): a 0.53-sec interval in FAC of perpendicular X component of the burst magnetic field, associated Wavelet power spectrum and whistler Poynting flux, respectively. (D) and (E): expanded views of the filtered whistler waveforms of the perpendicular X component of the burst magnetic field and the perpendicular Y component of the electric field over the time interval indicated by the purple bar in (A). (F): hodogram of the filtered burst magnetic field waveforms in FAC for the interval indicated by the green bar in (D). The black star and dot mark the beginning and ending of the wave field, respectively. (G) and (H): distribution functions of lower energy electrons (up to 20 keV) measured by ESA and higher energy electrons (20-700 keV) measured by SST observed at times close to the WH waves, respectively. The horizontal axis is parallel to the ambient magnetic field and the bulk velocity defines the plane.

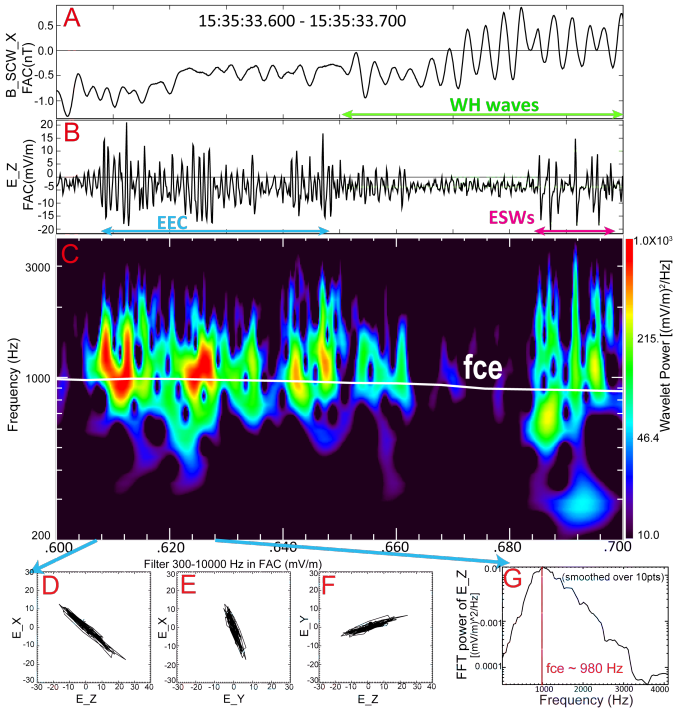

Figure 3. Example of electrostatic waves within the EDR. (A), (B) and (C): a 0.1-sec interval of the perpendicular X component of the burst magnetic field, the parallel Z component of the electric field waveform capture and the associated Wavelet power spectrum of the parallel electric field in FAC, respectively. (D), (E) and (F): hodograms of the electric field waveforms with an interval indicated by the light blue arrows below (C). The definitions of the black star and dot on hodograms are the same as those in Figure 2. (G): Fourier wave power vs. frequency with the same time interval as the hodograms.